JOURNAL OF THERMOPHYSICS AND HEAT TRANSFER
Vol. 25, No. 1, January–March 2011

Flowfield Uncertainty Analysis for Hypersonic Computational Fluid Dynamics Simulations

Andrew B. Weaver* and Alina A. Alexeenko†
Purdue University, West Lafayette, Indiana 47907
Robert B. Greendyke‡
Air Force Institute of Technology, Wright–Patterson Air Force Base, Ohio 45433
and
Jose A. Camberos§
U.S. Air Force Research Laboratory, Wright–Patterson Air Force Base, Ohio 45433

DOI: 10.2514/1.49522

Uncertainty quantification in the hypersonic flow regime offers valuable information to determine physical models in need of improvement and to assist in design of vehicles and flight experiments. Here we present results of uncertainty quantification analysis based on polynomial chaos method to determine flowfield and surface heat flux uncertainty under typical blunt-body reentry conditions. The NASA Langley Aerothermodynamic Upwind Relaxation Algorithm code [Cheatwood, F., and Gnoffo, P., "Manual for the Langley Aerothermodynamic Upwind Relaxation Algorithm (LAURA)," NASA TM 4674, 1996.], was used for axisymmetric computational fluid dynamics calculations of chemically-reacting, hypersonic flow over FIRE 2 configuration. A third-order polynomial chaos method using the Gauss–Hermite quadrature was applied for determining probability density functions and moments of output quantities. Input parameters such as freestream density, velocity, and temperature were varied, and the propagation of their corresponding uncertainties on output properties of interest through the flowfield were studied. The flowfield regions where the uncertainties are amplified due to nonlinear effects have been determined. An order of magnitude increase in surface heat flux uncertainties was observed for an input freestream velocity uncertainty of ±30 m/s, or 0.29%. This parameter thus has the greatest sensitivity to variations, and conversely the freestream temperature has the least sensitivity. The utility of analyzing higher moments, such as skewness, in addition to mean and deviation of the uncertain output parameters has also been demonstrated.

Nomenclature

a_k	=	deterministic coefficient of kth order
CV	=	coefficient of variation (relative uncertainty)
H_n	=	Hermite polynomial of order n
k	=	order of polynomial chaos expansion
m	=	number of dimensions
N	=	number of samples
n	=	order of accuracy for polynomial chaos expansion and Hermite polynomials
$\dot{q}$	=	heat flux, kW/m^2
T	=	translational temperature, K
V	=	velocity, m/s
w	=	weight corresponding to abscissa
x	=	input parameter value
Y	=	output value from solver
$\bar{Y}$	=	mean output value
γ	=	skewness
μ	=	mean
ξ	=	Gaussian random variable
ρ	=	density, kg/m^3
σ	=	standard deviation
Ψ	=	random basis function

Subscripts

i	=	collocation point index
ske	=	skewness

Presented as Paper 2010-1180 at the 48th AIAA Aerospace Sciences Meeting Including the New Horizons Forum and Aerospace Exposition, Orlando, FL, 4–7 January 2010; received 21 February 2010; revision received 8 October 2010; accepted for publication 14 October 2010.

*Graduate Student, School of Aeronautics and Astronautics.
†Assistant Professor, School of Aeronautics and Astronautics.
‡Associate Professor, Department of Aeronautics and Astronautics.
§Assistant to the Chief Scientist, Air Vehicles Directorate.

I. Introduction

THE development of advanced hypersonic aerospace vehicles remains a strong focus of several programs pursued by U.S. Air Force and NASA [1] as well as European agencies [2]. The design of hypersonic systems requires multidisciplinary studies involving structural mechanics, aerodynamics, propulsion and materials. Since both flight and on-the-ground experiments are expensive for hypersonic flight conditions, computational methods such as computational fluid dynamics (CFD) serve as critical tools in the analysis and design of such systems. While a deterministic CFD solution gives a single-point estimate for a fixed set of input parameters, in real-life hypersonic applications numerous uncertainties in the design, manufacture and operation must be addressed. With the modern computational capabilities it has become feasible to perform uncertainty quantification (UQ) analyses which are valuable to design processes. UQ indicates which parameters are contributing the most to the variability of an output quantity and introduces opportunities for design improvements.

One commonly encountered design challenge with hypersonic aerospace vehicles, and therefore an instance where UQ analysis is most useful, is that of aeroheating [3]. A large safety factor is typically assumed for the thermal protection system to account for uncertainties in predicted heating levels due to parameters such as reaction rates, transport properties, wall catalycity, internal energy relaxation rates, turbulence and laminar-turbulent transition models. This large safety factor results in excess material which affects overall mass and potentially the stability of the vehicle. By

quantifying the uncertainty levels expected during flight a more appropriate safety factor can be assumed.

Apart from the design of the vehicle itself UQ analyses can also prove useful in the design of experiments. With the high costs of both ground and flight testing the experiments must be designed to collect as much useful data as possible from a single test setup. A UQ analysis provides information about the flowfield which can then be used to place sensors in optimal locations. With these applications in mind, the purpose of this study is to provide an efficient method to quantify the uncertainties in flowfield properties of interest due to fluctuations in atmospheric conditions such as freestream temperature, density, and velocity as well as modeling parameters such as collision integral coefficients.

Monte Carlo (MC) random sampling methods is currently the most widely used approach for UQ analysis of CFD simulations due to its robustness and advantages for high-dimensional problems. Previous work by Palmer [4] had used the MC random sampling method to assess the sensitivities and uncertainties in crew exploration vehicle low Earth orbit and lunar return entries. The FIRE 2 vehicle experienced similar flight conditions to that of lunar return entries and thus was used in the study. The MC method is beneficial for high-dimensioned problems due to its convergence rate independence to the number of parameters, but it is still computationally expensive. To reach an adequate statistical error convergence, over 3000 CFD solutions were required from varying parameters such as dissociation/reaction rates, exchange/ionization reaction rates, vibration-dissociation coupling, *V-T* relaxation time, and binary collision integral. Of these, it was determined that the N_2-N collision integral contributed the most to the heating rate uncertainty. MC random sampling is the most widely used tool, but more recently developed methods show promise towards reducing the computational costs while maintaining a high level of accuracy.

Polynomial chaos (PC) methods which use deterministic sampling reduce the number of samples required [5] and are therefore attractive for three-dimensional CFD analyses. Hosder and Walters [6] describe various PC methods and how to implement them into fluid dynamics problems. The crux of the method is to project the output quantity onto an orthogonal basis which can be implemented either nonintrusively at the run-level or integrated into the solver.

One downside of the deterministic sampling methods has been the curse of dimensionality; which limits its use to studying only a few parameters simultaneously. To extend this approach to higher dimensional cases, a sparse-quadrature method can be used instead as described by Nobile et al. [7]. More recently, Witteveen and Iaccarino [8] have developed a multi-element stochastic collocation method which refines one element at a time until a final convergence criteria is met. Either of these two approaches could be implemented into a higher dimensional uncertainty analysis to improve convergence rates.

It is important to note two categories of uncertainty encountered in CFD. The aleatory uncertainty is the uncertainty originating from the variability of input parameters, such as the freestream atmospheric properties. For such aleatoric variables, a probability distribution function (PDF) can be constructed based upon existing data of sufficient number of samples. The number of samples is emphasized because in order to accurately predict the input uncertainty, the frequency of parametric values in a particular interval should be recorded. An example of aleatoric uncertainty is fluctuations in Earth atmospheric density. Champion [9] reports, for example, fluctuations in Earth atmospheric density of $\pm 5\%$ between 48 and 69 km and $+4\%$ to -16% between 70 and 80 km. Often times, one must rely on searching through literature or expert opinion for such input uncertainty estimates rather than sufficient experimental data. This leads to another type of uncertainty, which is termed epistemic. This uncertainty is originated from a lack of knowledge of the true value of the metric of interest. Roy and Oberkampf [10] state two approaches to represent epistemic uncertainty. The first is to define a PDF based upon the degree of belief of the analyst rather than the frequency of occurrence as defined for aleatoric uncertainty. The second approach is to represent the uncertainty as an interval-valued quantity such that no value is more probable than the next. Their study demonstrates how both types of uncertainties may be propagated through the model.

For the current study, mostly the aleatoric uncertainties are considered, in particular, for the atmospheric freestream flow parameters. The remainder of the paper is organized as follows. Section II describes the CFD simulations approach and the polynomial chaos expansion (PCE) procedure. Section III presents the verification of the PCE reconstruction of PDF and its moments for the cases of Fay–Riddell heat flux correlation and flowfield temperature from FIRE 2 experiment. Results of UQ analysis are presented and discussed in Sec. IV.

II. Simulation Approach

In this study the deterministic UQ analysis is being performed for uncertainties in CFD model parameters such as binary collision integrals as well as atmospheric freestream flow parameters. This section describes how the CFD simulations were setup and presents the PC expansion methodology as it was applied in the current study.

A. CFD Case Setup

All cases were solved using the NASA Langley Aerothermodynamic Upwind Relaxation Algorithm (LAURA); which is a nonequilibrium, chemically-reacting, Navier–Stokes solver. Point-relaxation and convergence criteria of 5×10^{-12} were used since surface heating is the last quantity to converge. A baseline case was considered using the forebody of the FIRE 2 geometry and flow conditions corresponding to the 1643 s, peak heating trajectory point. The geometry of the FIRE 2 vehicle was specified in the NASA TM X-1305 [11] report, and is shown in Fig. 1 for reference. The FIRE 2 capsule had three beryllium heat-shields that were exposed at different times during the reentry to provide a clean measurement interval. The current study focuses on the peak heating rate and at which time the second beryllium shield is being used. Therefore the geometry specifications were taken according to the second experimental period, but only for the forebody.

The freestream conditions including species molar concentrations based on standard atmosphere data for the given altitude of 53.04 km at 1643 s are $\rho = 7.8 \times 10^{-4}$, $V = 10,480$, $T = 276$, $N_2 = 0.737795$, and $O_2 = 0.262205$. At these conditions significant ionization occurs and so the 11-species air model was used (N_2, O_2, NO, N, O, N^+, O^+, NO^+, e^-, $N_2{}^+$, $O_2{}^+$).

The FIRE 2 vehicle had reentered at an angle of attack of nearly zero, and therefore an axisymmetric boundary condition was applied. Based on work done by Palmer [4], who had reported a good agreement with experimental data [11], the wall was assumed to be noncatalytic to neutrals and fully-catalytic to ions with a constant temperature of 640 K. A radiative equilibrium wall boundary con-

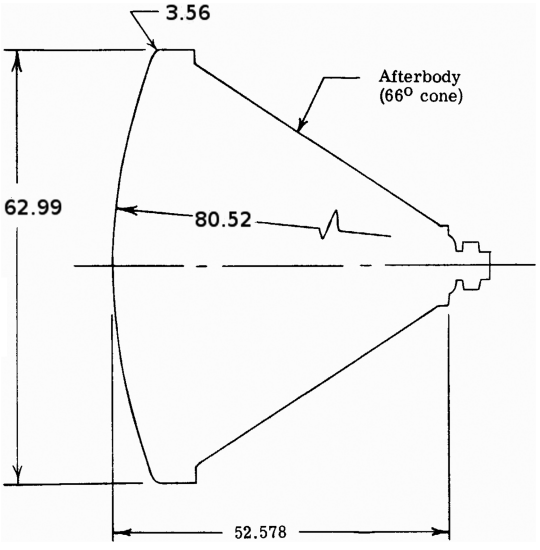

Fig. 1 FIRE 2 geometry. All dimensions are in cm.

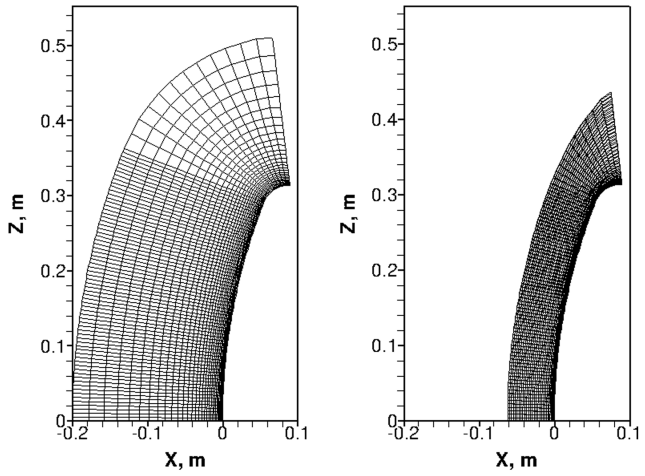

a) Initial grid **b) Final grid after adaptation and alignment**

Fig. 2 Structured grid of axisymmetric FIRE 2 forebody.

dition would be more realistic, and is another area worth studying. The initial, structured grid used for the computations is shown in Fig. 2a, and the final grid after adaptations and shock alignments is shown in Fig. 2b.

B. PCE Methodology

Input parameters were assumed to have Gaussian PDF's as in the analysis by Palmer [4]. The statistical moments such as mean, standard deviation, and skewness of output properties were calculated by using Gauss–Hermite quadrature. This integration method approximates the continuous, Gaussian-distributed function as a sum of finite terms as expressed in Eq. (1):

$$\int_{-\infty}^{+\infty} f(x)e^{-x^2}\,\mathrm{d}x \approx \sum_{i=1}^{n} f(x_i)w(x_i) \tag{1}$$

The summation in the previous equation contains n collocation points, the function of Hermite polynomials and the random variables, $f(x)$, and the weighting function, w, corresponding to the Gaussian distribution.

Determination of the collocation points is done by first solving the zeros (abscissas) of the Hermite polynomials [12,13], which are tabulated to fifth order in Table 1. By using the abscissas in an inverse form of the normal distribution the collocation points can be computed. Using the abscissas of the order of accuracy desired and the statistical parameters of the input PDF, the input parameter values for Gauss–Hermite quadrature can be determined as

Table 1 Hermite polynomials and corresponding zeros up to fifth order

Hermite polynomials	Zeros
$H_0(\xi) = 1$	——
$H_1(\xi) = 2\xi$	0
$H_2(\xi) = 4\xi^2 - 2$	± 0.70710678
$H_3(\xi) = 8\xi^3 - 12\xi$	$0, \pm 1.2247449$
$H_4(\xi) = 16\xi^4 - 48\xi^2 + 12$	$\pm 1.6506801, \pm 0.52464762$
$H_5(\xi) = 32\xi^5 - 160\xi^3 + 120\xi$	$0, \pm 2.0201829, \pm 0.95857246$

$$x_i = \mu + \sqrt{2}\sigma\xi_i \tag{2}$$

where for a given input parameter, x_i is the input parameter value corresponding to the roots of the Hermite polynomials, ξ_i, and μ and σ are the mean and standard deviation of the input PDF, respectively.

The weights corresponding to the abscissas are determined from Eq. (3). These weights will then be used in the PCE in order to construct the output PDF as well as for the calculation of moments of output quantities within the flowfield:

$$w_i = \frac{2^{n-1}n!}{n^2[H_{n-1}(\xi_i)]^2} \tag{3}$$

The subscript, $(n-1)$, implies the Hermite polynomial corresponding to the $(n-1)$ order.

For an output quantity, Y, such as temperature, pressure, surface heat flux, etc., the mean value may be computed as follows:

$$\bar{Y} = \sum_{i=1}^{n} w_i Y(x_i) \tag{4}$$

Similarly, the standard deviation, σ, may be computed as defined in Eq. (5):

$$\sigma = \sqrt{\sum_{i=1}^{n} w_i (Y(x_i) - \bar{Y})^2} \tag{5}$$

The relative uncertainty, or coefficient of variation (CV), is a second-order, central moment and is calculated as follows:

$$\mathrm{CV} = \frac{\sigma}{\bar{Y}} \tag{6}$$

Skewness, γ, is a third-order, central moment which is defined as

$$\gamma = \left(\frac{\sum_{i=1}^{n} [w_i (Y(x_i) - \bar{Y})^3]}{\sigma^3} \right) \tag{7}$$

The stochastic variable may be found from the deterministic component as expressed in the PC expansion next:

$$Y = \sum_{k=0}^{n} a_k \Psi_k(\xi) \tag{8}$$

where a_k is the deterministic coefficient of kth order ($k = 0, 1, \ldots, n$) and Ψ_k is the random basis function of kth order (note for the Gauss–Hermite quadrature used in this analysis Ψ corresponds to the Hermite polynomials, H). To construct the output PDF of a particular flowfield property, the procedure listed next was used:

1) First solve for the deterministic coefficients, a_k, using the output values from the solver. The relation between the sampled output and deterministic coefficient values are given in Eq. (9):

$$\langle Y, \Psi_k \rangle = \left\langle \sum_{i=0}^{n} a_i \Psi_i, \Psi_k \right\rangle \tag{9}$$

Because of the orthogonality of the Hermite polynomials the inner product of the random basis function is equal to zero for $n \neq k$, or $\langle \Psi_n, \Psi_k \rangle = \langle \Psi_n, \Psi_k \rangle \delta_{nk}$. Equation (9) then becomes

Table 2 Moments of Fay–Riddell stagnation point heat flux calculated using MC sampling with varying sample size, N

	$N = 10^5$			$N = 10^6$			$N = 10^7$		
M_∞	$\dot{q}_{\mathrm{mean}}$	CV,%	$\dot{q}_{\mathrm{ske}}$	$\dot{q}_{\mathrm{mean}}$	CV,%	$\dot{q}_{\mathrm{ske}}$	$\dot{q}_{\mathrm{mean}}$	CV,%	$\dot{q}_{\mathrm{ske}}$
3	54.20	22.125	0.2551	54.20	22.074	0.2509	54.20	22.085	0.2515
7	894.56	17.677	0.2164	894.48	17.635	0.2124	894.51	17.654	0.2126

$$a_k = \frac{\langle Y, \Psi_k \rangle}{\langle \Psi_k^2 \rangle} = \frac{1}{\langle \Psi_k^2 \rangle} \sum_{i=1}^{n} Y(x_i) \Psi_k(\xi_i) w_i \tag{10}$$

where for the current study, n is three so that a third-order PCE is obtained. This follows from the more general expression given by Najm [14] which applies to multidimensions. It is referenced here in Eq. (11):

$$a_k = \frac{1}{\langle \Psi_k^2 \rangle} \sum_{i_1=1}^{n} \cdots \sum_{i_m=1}^{n} Y(x_{i_1}, \ldots, x_{i_m}) \Psi_k(\xi_{i_1}, \ldots, \xi_{i_m}) \prod_{k=1}^{m} w_{ik} \tag{11}$$

2) Generate samples, ξ, from a normal distribution with a mean equal to zero and a standard deviation equal to $1/\sqrt{2}$.

3) Using the coefficients calculated in Eq. (11) compute the PC expansion for each sample, ξ, as defined next in Eq. (12):

$$Y = \sum_{k=0}^{n} a_k \Psi_k(\xi) \tag{12}$$

Hypersonic environments can have significant nonlinearity effects between parameters and so higher dimensioned cases should be studied as well. The preceding methods were implemented in the verification and uncertainty analyses to follow.

III. PC Verification

Two cases were considered for verification of PC approach. The first is the surface heat flux computed by the Fay–Riddell stagnation point heating correlation. For this case, the PC solutions were compared with those obtained using the MC random sampling. The mean, relative uncertainty, and skewness from both PC and MC methods are compared for two Mach numbers. Results from this case are presented in Sec. III.A. Second, we consider the PC convergence of the relative uncertainty in translational temperature from the FIRE 2 experiment. Relative uncertainties are compared for second-, third-, and fourth-order PC expansions.

A. Fay–Riddell Stagnation Point Heating PC Convergence

A stagnation point heat flux analysis has been performed on a hemisphere using the Fay–Riddell correlation for varying freestream temperature and at several Mach numbers. The purpose for this particular analysis is to verify the implementation of the PC approach. A satisfactory order of accuracy in the PCE will also be assessed from this.

The mean, relative uncertainty, and skewness are calculated for both MC and PC methods and are shown in Tables 2 and 3, respectively. Increasing the number of samples used in the MC method has decreasing effects on the statistical moments. This trend is also true for increasing the order of accuracy used in the PC method. Beyond third order the statistical moments remain unchanged, and therefore third-order PCE will suffice.

Two additional observations can be made from this verification case. One is the inability to accurately calculate the skewness present in the surface heat flux for second-order PC method. Noting that skewness is a third moment, it is clear that a second-order function will not be able to predict skewness and thus is the case. The other observation is the uncertainty in heat flux due to ±10% variation in freestream temperature variation tends to decrease with increasing Mach number. Thus, at high Mach numbers the effect of freestream temperature variation on the surface heat flux is expected to be less significant.

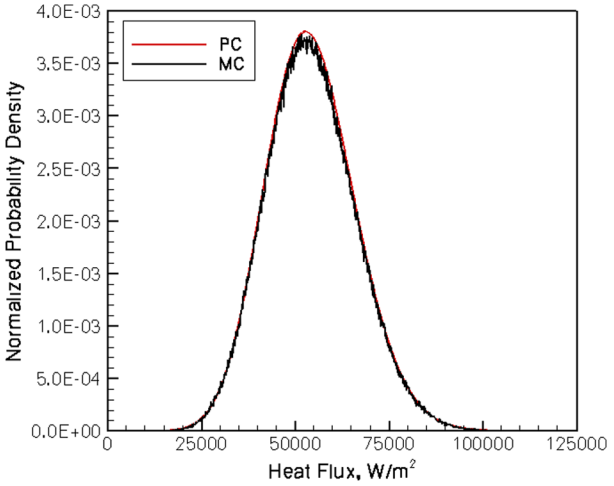

a) Comparison between MC and PC methods for $M_\infty = 3$

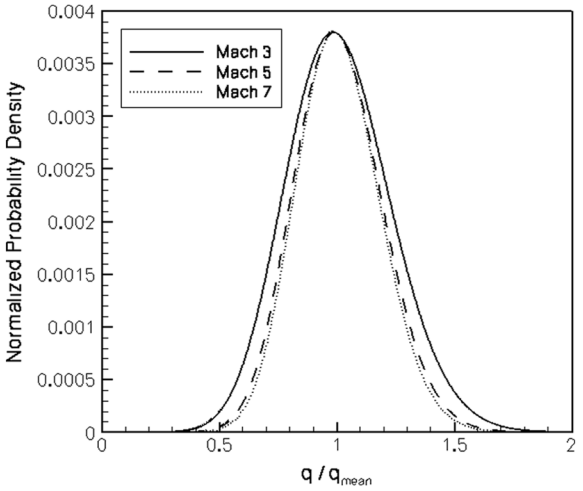

b) Mach number effects on PDF

Fig. 3 Fay–Riddell stagnation point heat flux.

A third-order PCE was used to construct the stagnation point heat flux PDF and was compared with the PDF constructed using the MC method. The MC method used one million samples and from Fig. 3a it is clear that there is a good agreement. The Mach number effects on the heat flux PDF as calculated via the PC method is shown in Fig. 3b. Although the standard deviation is undoubtedly larger for the higher Mach number, the mean increases at a larger rate than the standard deviation resulting in the lower level of uncertainty as already discussed.

It is worthwhile to note that skewness is indicating nonlinearity in the output properties due to input variations. A skewness of zero would indicate a linear dependence on the input parameter. It is also useful to establish a scaling by comparing the skewness to that of known PDFs. One such PDF is the Maxwell–Boltzmann distribution, and it was determined that this distribution has a skewness of approximately 0.4857. This value will be the scaling to distinguish

Table 3 Moments of Fay–Riddell stagnation point heat flux calculated using PC expansion with varying order, n

	$n=2$			$n=3$			$n=4$		
M_∞	$\dot{q}_{\text{mean}}$	CV,%	$\dot{q}_{\text{ske}}$	$\dot{q}_{\text{mean}}$	CV,%	$\dot{q}_{\text{ske}}$	$\dot{q}_{\text{mean}}$	CV,%	$\dot{q}_{\text{ske}}$
3	54.20	22.076	1.2062×10^{-15}	54.20	22.091	0.2522	54.20	22.091	0.2522
7	894.49	17.642	1.3640×10^{-15}	894.50	17.649	0.2136	894.50	17.649	0.2136

Table 4 FIRE 2 PC convergence for translational temperature

PC order	Preshock CV, %	Postshock CV, %	L2 norm, μ	L2 norm, σ
$n = 2$	3.9618	3.9600	–	–
$n = 3$	3.9175	4.0290	2.722×10^{-4}	4.014×10^{-2}
$n = 4$	3.9883	4.0221	1.301×10^{-4}	1.120×10^{-2}

high and low skewness in the surface heat fluxes discussed in the next section.

B. PC Convergence for FIRE 2 Flow

Verification of the use of a third-order PC expansion for flowfield properties from the FIRE 2 experiment is presented in this section. The flow conditions are given in Sec. II.A, and for the purposes of verification, only the translational temperature is being analyzed from the freestream density variation case described in Sec. IV.B. For this verification, the convergence of second-, third-, and fourth-order PC expansions are determined by the observations of the CV and L2 norms of the mean temperature and standard deviation of temperature. These results are presented in Table 4. Also note that the CV is recorded at pre and postshock locations along the stagnation streamline.

Results in Table 4 show that for increases in PC order the L2 norms of the mean temperature and standard deviation of temperature are converging. It also demonstrates that only small improvements are attainable with fourth-order with respect to third-order.

IV. Results and Discussion

Here we consider effects of model uncertainties on distributed quantities such as surface heat flux and distributions of flow properties such as fields of temperature, pressure, and species concentrations. The input variance for each parameter is given in Table 5. The estimated uncertainties for all parameters were taken from Palmer [4] except for the freestream velocity, which was based on uncertainty reported by Hillje [16].

A. Grid Convergence Study

A grid convergence study was performed to ensure that a sufficiently resolved grid was used. The grid was refined in the normal direction to a size of 82 streamwise x 128 normal to the body. Note for the remainder of the paper the specification of grid size will always be the streamwise value followed by the normal value. At the stagnation point, the refined grid resulted in a 0.02% higher surface heat flux. This difference increased to a maximum difference of 1.34% at a location nearly halfway around the body.

In comparison to the stagnation heat flux reported by Palmer [4] the current simulations are nearly 5.5% lower. Part of this difference can be attributed to the differences in the codes used (DPLR vs LAURA). A code verification study performed by Hash et al. [17] had compared peak surface heating on the FIRE 2 vehicle for DPLR, LAURA, and US3D codes. This study had reported LAURA simulations to have approximately 2% less stagnation point surface heating than DPLR simulations. The reasoning for the remaining differences is unclear, however, for the purposes of analyzing uncertainties in the flowfield properties (which are computed from the baseline case) the current results are acceptable. Figure 4 shows the surface heat flux as a function of grid size.

Table 5 Estimated uncertainties of input parameters

Parameter	Description	Uncertainty
V_∞	Freestream velocity	± 30 m/s
ρ_∞	Freestream density	$\pm 10\%$
$D1$, $D2$	Collision integral coefficients [a]	$\pm 30\%$
T_∞	Freestream translational temperature	$\pm 10\%$

[a]Collision integrals are given in the form given by [15].

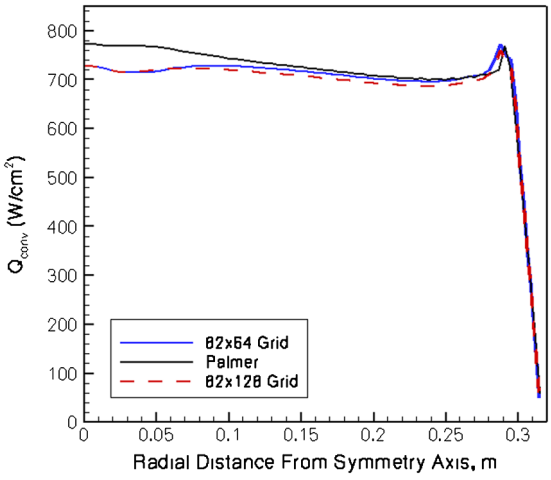

Fig. 4 Grid convergence.

Following from this analysis it was determined that the 82×64 grid would suffice for computing the flowfield properties and therefore was used in all UQ simulations. The translational temperature and static pressure contours for the baseline case are shown in Figs. 5a and 5b, respectively.

All UQ results being presented have been obtained using the same adapted, baseline grid, and as such could potentially introduce a source of error. To determine the effect that grid adaptation has on the output properties of interest the freestream density variation case was further examined. The baseline grid and solution was restarted for a -10% variation in freestream density as is done in the UQ analysis, but here the grid was allowed to adapt. Surface heat flux and translational temperature profiles across the shock show small differences in magnitude in comparison to the case using the baseline grid. In Fig. 6a the translational temperature for the current, adapted grid has nearly the same peak value but at a location approximately 2 mm before the baseline grid. The surface heat fluxes shown in Fig. 6b have differences on the order of 0.1% for all locations except for those in the region from 0.02–0.07 m, where the differences are approximately 1.4%. As will be discussed in the next section on freestream density variations, the uncertainty in surface heat flux within this region is approximately 6%, and so at most the grid adaptation effects account for 1/4 of the uncertainty percentage.

B. Freestream Density Variation

Next, the effect of Gaussian input uncertainty in freestream density on the flowfield properties is considered. Figures 7a and 7b show the uncertainties in translational temperature and static pressure within the flowfield, respectively. Note the regions of greatest uncertainty in temperature for an input 10% uncertainty in freestream density are: before and after the shock and in the expansion region around the shoulder.

After the shock there exists a peak in translational temperature as seen in Fig. 8 and hence leads to high uncertainty. This peak in the translational temperature occurs across the shock due to the initial gradients in flowfield properties across a shock and the following loss of kinetic energy to dissociate the nitrogen and oxygen molecules. Also, observe the decrease in uncertainty in the vicinity of the shock as it forms around the body.

Uncertainties in the static pressures have nearly the same maximum value of 4% as for the translational temperature, however, the distribution within the flowfield is different. For the static pressures, the global maximum uncertainty is located in the shoulder expansion region in the shock. Note in Fig. 7b the uncertainty is nearly the same as for translational temperature ahead of the shock, but after the shock the uncertainty is much less. The static pressure has no peak like seen for temperature, and so the maximum uncertainty is where the static pressure is least. Differences in static pressure around the shoulder region for the three freestream density cases are somewhat smaller than those seen along the stagnation

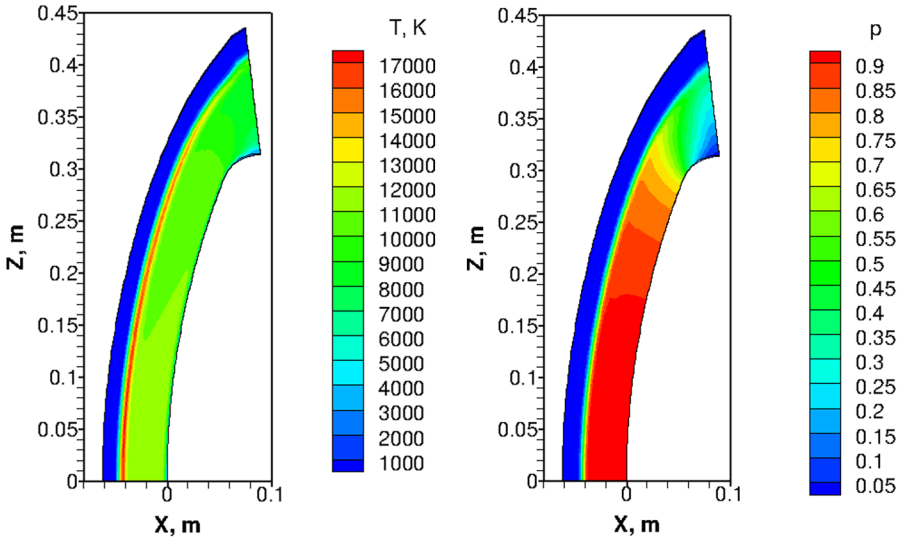

a) Translational temperature contour **b) Normalized static pressure contour**

Fig. 5 Flowfield contours for baseline case.

streamline, but the pressures are low enough that the percent differences are greater.

A 10% variation in freestream density has a larger effect on surface heat flux with a maximum value of nearly 8.5% within the shoulder region. This is only slightly larger than at the stagnation point, which has an uncertainty of 8%. Figures 9a and 9b show the surface heat flux for the three density variation simulations and their corresponding uncertainties due to variation in freestream density, respectively.

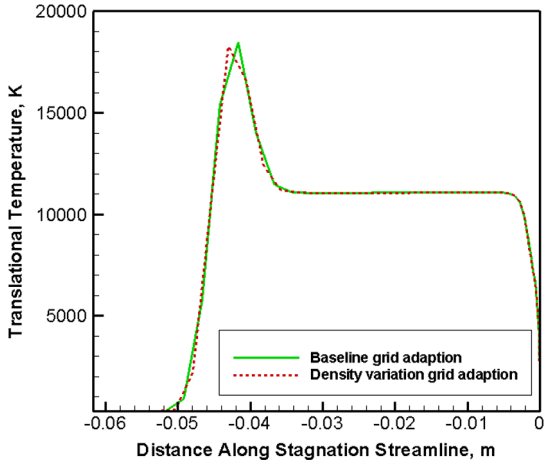

a) Translational temperature

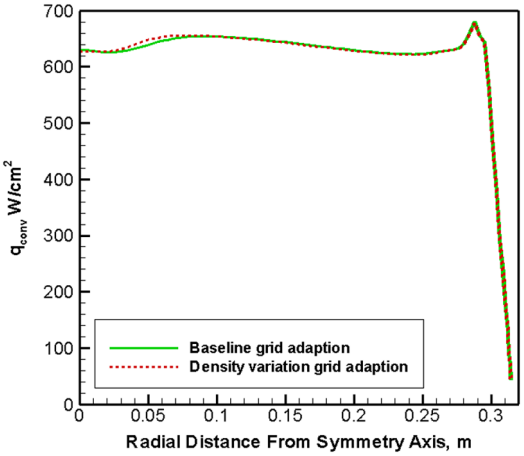

b) Surface heat flux

Fig. 6 Effect of grid adaptation on output properties.

Varying the freestream density has a significant effect on the boundary-layer thickness, and which in turn is effecting the surface heating rates through the shear stresses at the wall. The boundary-layer thicknesses decrease with increasing densities, and vice versa. As would be expected, the shear stresses at the wall increase with an increase in freestream density. Computing the differences in boundary-layer thicknesses shown in Fig. 10 show nearly identical results as for the surface heating uncertainty, indicating this to be the main contributing source.

Negative skewness in surface heat flux has been calculated for the entire surface, and is shown in Fig. 9b. The skewness varies from nearly -0.3 at the stagnation point to -0.8 at the outflow of the shoulder region, and this shows that mean surface heat fluxes are underpredicted most significantly in the shoulder region.

C. Freestream Temperature Variation

Here, the effect of Gaussian input uncertainty in freestream temperature on the flowfield properties is considered. Figures 11a and 11b show the uncertainties in translational temperature and static pressure within the flowfield, respectively. Clearly, a variation in freestream temperature by $\pm 10\%$ should result in a 10% relative uncertainty in the translational temperature in the freestream. This is indeed the case, and since pressure is directly related to temperature the pressure also experiences a 10% relative uncertainty in the freestream.

After the bow shock the uncertainty levels decrease by 2 orders of magnitude. If, however, the wall were assumed to be in radiative equilibrium and a finite catalytic efficiency the uncertainty in the boundary layer would be expected to be more significant.

The surface heat flux uncertainty is a maximum at the stagnation point with a value slightly less than 0.25. This is only 2.5% of the input uncertainty and as such is insignificant. This trend was inferred from the PC verification in Sec. IV.A but is confirmed here. Figures 12a and 12b illustrate the surface heat fluxes and their relative uncertainties, respectively.

D. Freestream Velocity Variation

The hypersonic flowfield is sensitive to the variation in freestream velocity. For an estimated Gaussian input uncertainty in freestream velocity of 0.29% the flowfield properties vary by more than 4.8% at their maximums. Figures 13a and 13b show the uncertainties in translational temperature and static pressure, respectively.

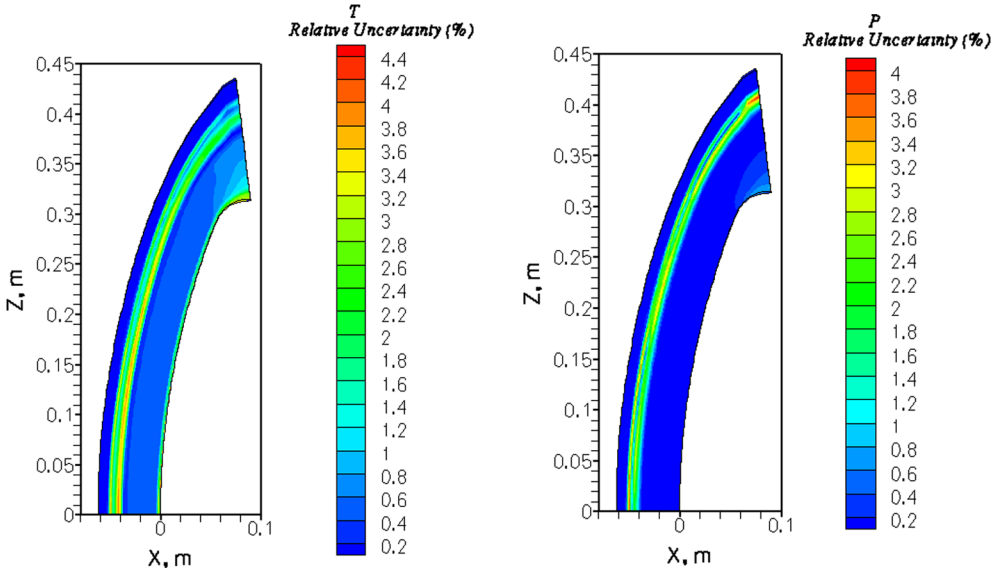

a) Translational temperature **b) Static pressure**

Fig. 7 Uncertainty quantification in flowfield because of density variation (%).

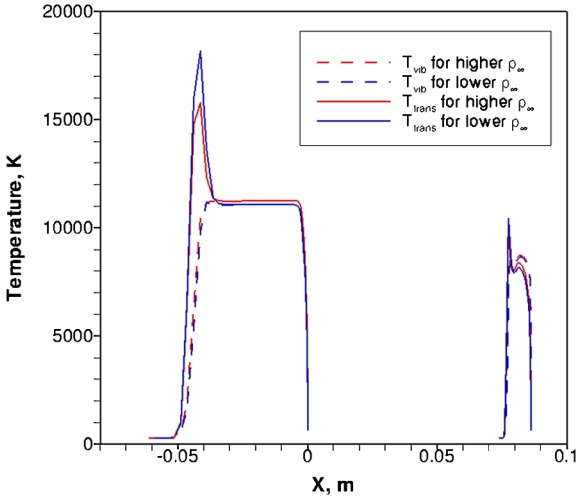

Fig. 8 Translational temperature across shock in both stagnation and shoulder regions.

The global maximum uncertainty is located within the shock in the shoulder expansion region, and the uncertainty increases with increasing distance from the symmetry axis, Z.

Comparisons between the surface heat flux from the mean input velocity with the mean of the surface heat fluxes show more significant differences here than in the previous case with density variations. This can be seen in Fig. 14a. The uncertainties in surface heat flux were also strongly affected, with an estimated input uncertainty of 0.29%, the surface heat flux uncertainty has a maximum value of 2.6%. The uncertainty in surface heat flux decreases a short distance from the stagnation point, but increases rapidly in the shoulder region to the maximum of 2.6%, as shown in Fig. 14b.

As can be seen in Fig. 10, the boundary-layer thickness grows rapidly in the shoulder expansion region. This has the effect of rapidly decreasing the velocity gradient. The velocity profile becomes more full with increasing velocities, and as such increases the shear stresses at the wall. At the stagnation point the velocity gradient is small, and a small variation in freestream velocity results in a larger percent difference in the velocity gradient. As the air flows around the surface the velocity gradient increases, but since this increase will be similar for each case the percent difference is less. Once the air flows around the shoulder the velocity gradient

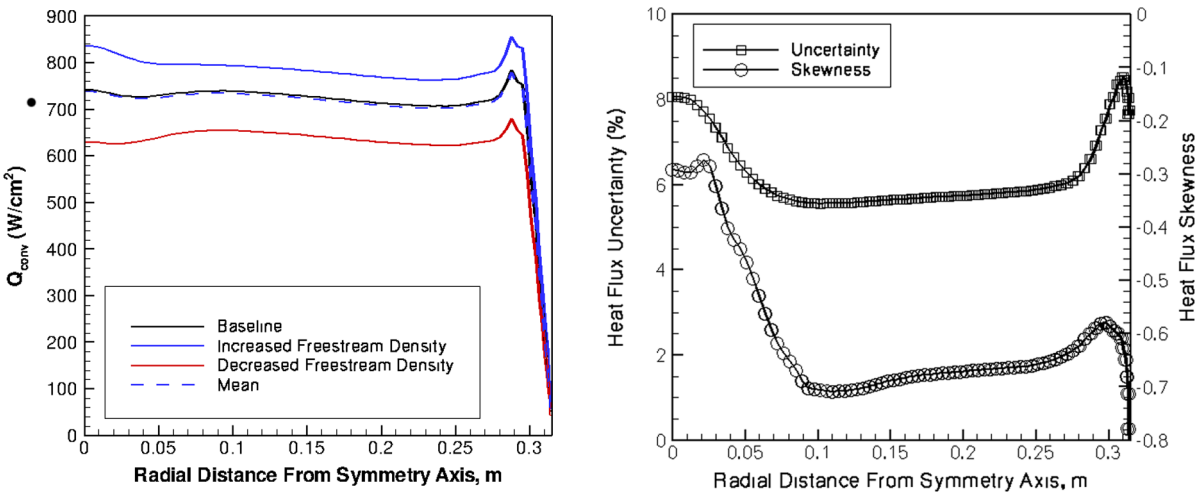

a) Surface heat flux comparison **b) Surface heat flux uncertainty**

Fig. 9 Surface heat flux variations because of density variation (%).

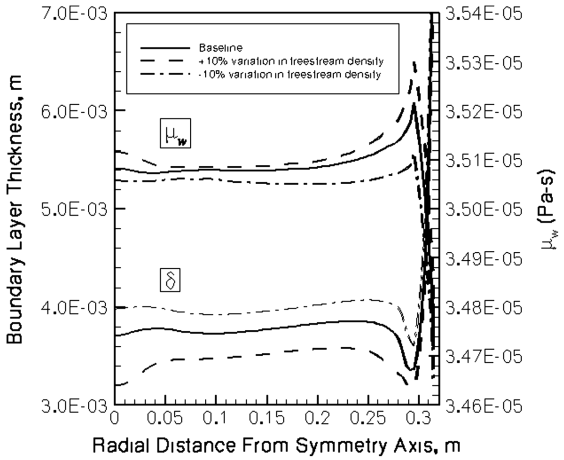

Fig. 10 Freestream density variation effects on boundary-layer thickness.

decreases, and as before the small variation in freestream velocity causes larger variation in surface heat flux.

A relatively constant, positive skewness in surface heat flux was computed over the surface. The skewness of 1.1 due to freestream velocity variations is larger in magnitude than for freestream density variations but here is a positive value. This shows that for freestream density variations the mean surface heat flux is an over-prediction.

E. Collision Integral Coefficient Variation

Varying the collision integral coefficients effectively varies the transport properties (diffusivity, viscosity, and thermal conductivity) of the gas species. The effect of a Gaussian input 30% variation in collision integral coefficients on the uncertainty in translational temperature and static pressure is shown in Figs. 15a and 15b, respectively. Uncertainties are greatest within the boundary layer where the concentration of N and N_2 pairs is also greatest. Relatively high uncertainties are found in the expansion around the shoulder as shown in Fig. 15a, but this uncertainty lies within the boundary layer and that of which particles are able to expand. A decrease in uncertainty is observable as the wall is approached.

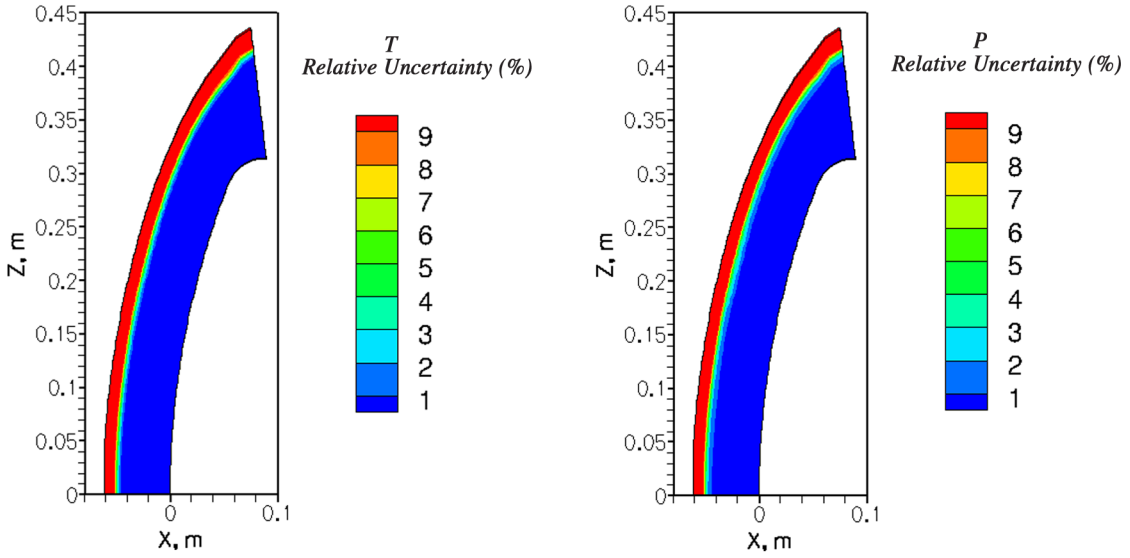

a) Translational temperature **b) Static pressure**

Fig. 11 Uncertainty quantification in flowfield because of temperature variation (%).

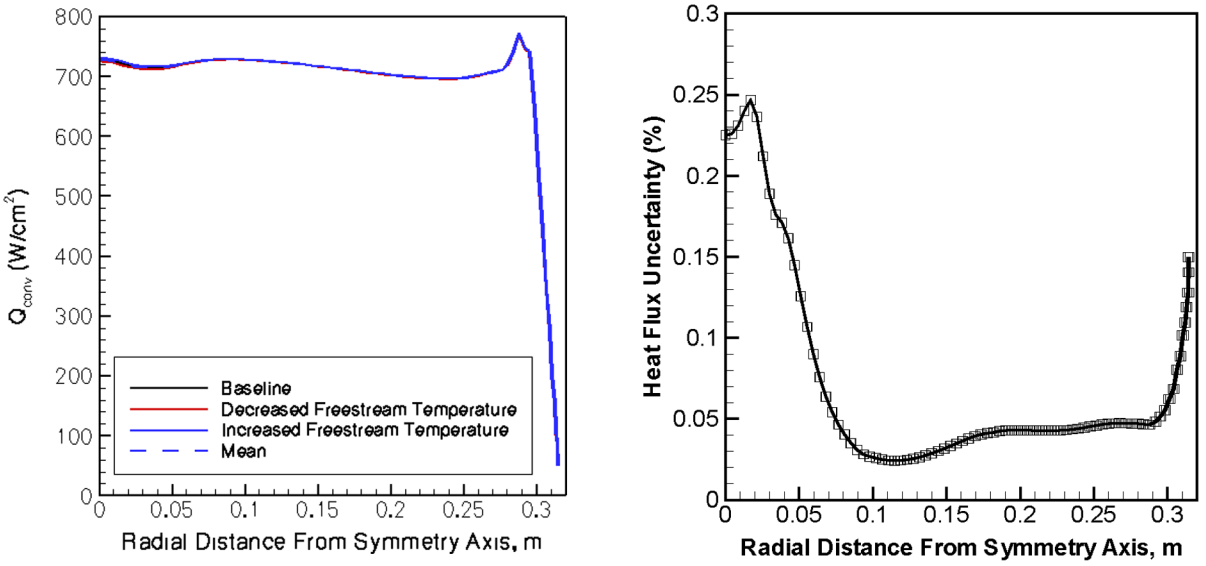

a) Surface heat flux comparison **b) Surface heat flux uncertainty**

Fig. 12 Surface heat flux variations because of temperature variation (%).

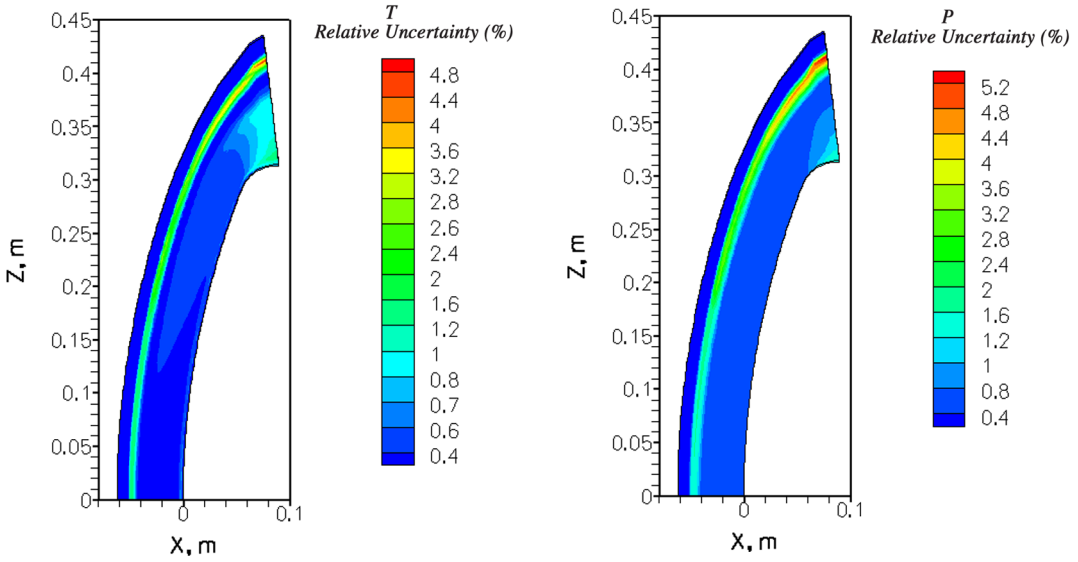

a) Translational temperature **b) Static pressure**

Fig. 13 Uncertainty in flowfield because of velocity variation (%).

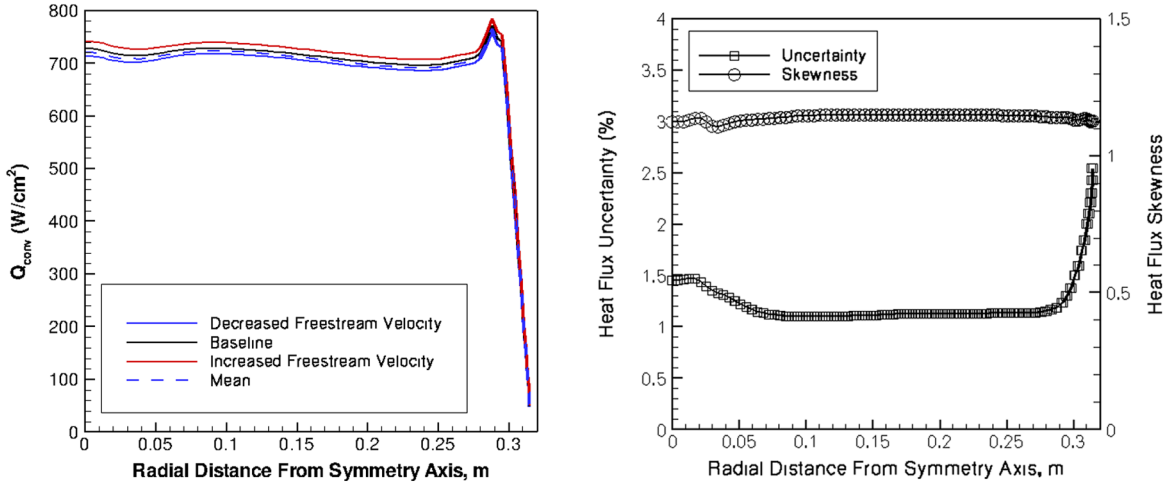

a) Surface heat flux comparison **b) Surface heat flux uncertainty**

Fig. 14 Surface heat flux variations because of freestream velocity variations.

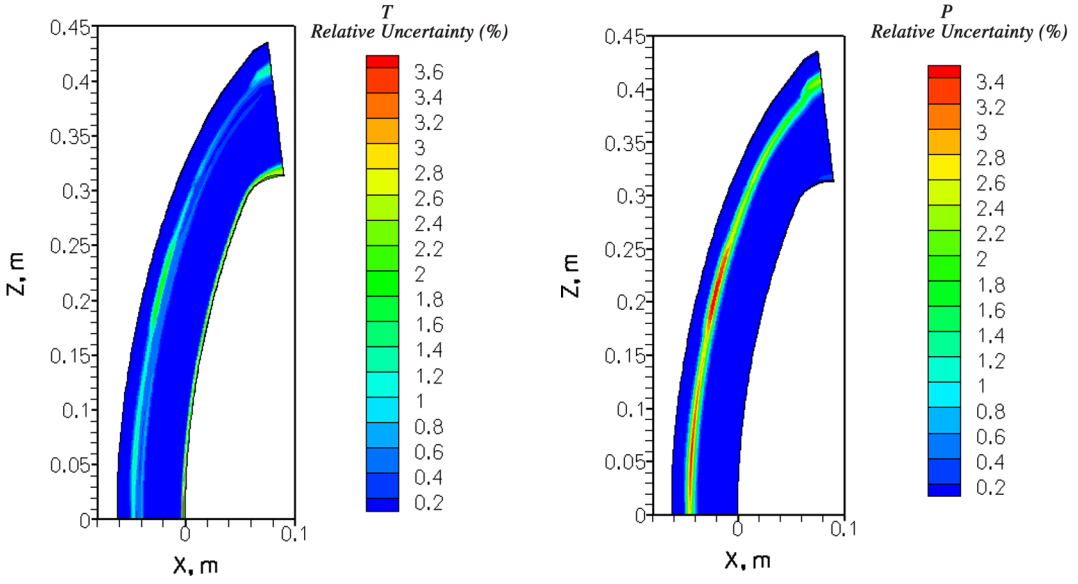

a) Translational temperature **b) Static pressure**

Fig. 15 Uncertainty in flowfield because of collision integral coefficient variation.

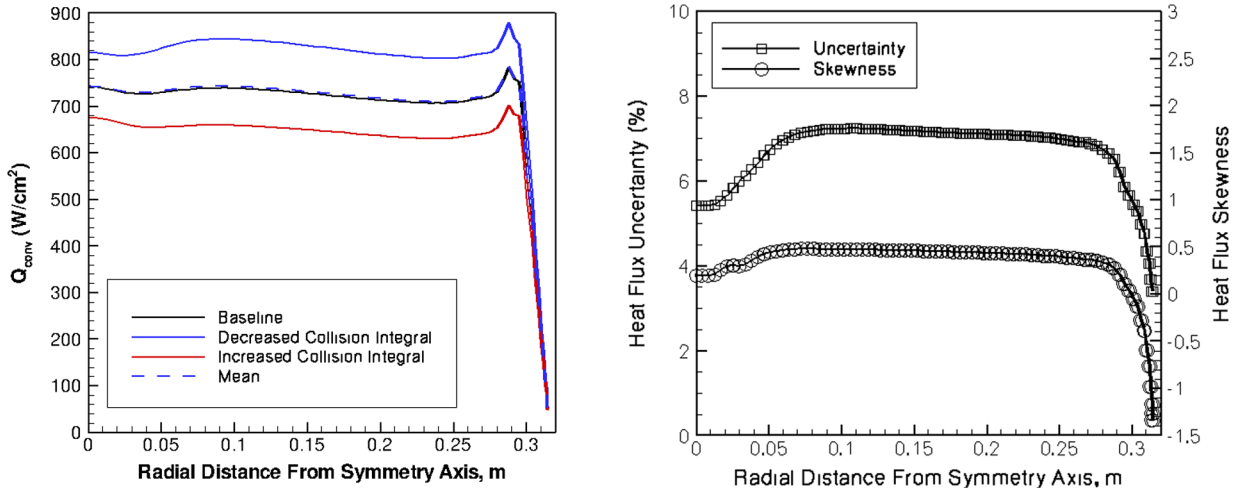

a) Surface heat flux comparison **b) Uncertainty in surface heat flux**

Fig. 16 Surface heat flux variations because of collision integral coefficient variations.

From the 30% estimated input uncertainty the maximum uncertainty in surface heat flux was about 7.3% located in the region between the stagnation point and the shoulder. The uncertainty starts at a local minimum of 5.5% at the stagnation point and increases to the maximum value, where it remains nearly constant until the shoulder region. In the shoulder region the uncertainty decreases rapidly to a value less than 4% at the last point. As with the previous cases, the surface heat flux from the mean collision integral value was compared with the mean of the surface heat fluxes. The results show that there is good agreement with only slight deviations between the stagnation point and shoulder regions. Figures 16a and 16b show the surface heat fluxes and their corresponding uncertainties for the variations in collision integral coefficients, respectively.

The uncertainty drops rapidly in the shoulder region and this is due to the decrease in molecules through the expansion. Because less collisions will occur in this region, varying the collision integral will not have as much effect on heat transfer as in areas of high number densities (such as the stagnation point). The variation in concentrations for dissociated species results in variations in boundary-layer thicknesses owing to the higher compressibility of a dissociated gas. Since only one collision pair out of all possible collisions is being varied, it is possible to be observing lower sensitivities to this parameter in comparison with Palmer [4] whose study had included variations for all collision pairs. It should also be noted that here an input uncertainty of 30% for the N_2-N collision integral is being used, whereas Palmer [4] had used 30% for all collision pairs with the exception of: N_2-N, N_2-O, and N-O. Palmer [4] had reported the N_2-N, N_2-O, and N-O collision integrals to account for approximately 76% of the overall sensitivity, it may be necessary to account for the nonlinear effects. Multidimensions may be employed in the PCE methodology outlined in Section II.B albeit at a cost. The total number of collocation points, P, required grows exponentially: $P = (k+1)^m$. This implies that integration of the three-dimensional problem desired (while maintaining third-order expansions) 64 collocation points would be needed. To combat this high computational cost with increasing dimensions, the sparse-quadrature method [7] can be implemented.

Skewness in surface heat flux due to N_2-N collision integral coefficient variation is shown in Fig. 16b to vary from approximately 0.2 at the stagnation point to -1.3 at the outflow of the shoulder region. Interestingly, the skewness switches sign at a location 0.3 meters away from the symmetry axis and which corresponds to the point where the flow begins to accelerate over the shoulder. This and the freestream temperature are the only parameters which had produced a sign change in skewness, and it is also important to note the maximum magnitude in skewness is greater for this parameter than either of the other three parameters.

The stagnation point heating values are used to construct a PDF for varying collision integral coefficients and is shown in Fig. 17. The PDF is positively skewed with a value of 0.1953, which implies that the surface heating is more responsive to a decrease in the collision integral coefficient. The corresponding mean and standard deviation as calculated from the PDF are 742.78 and 40.36 W/cm^2, respectively.

To help visualize the skewness in the output PDF, a symmetric PDF possessing the same mean and standard deviation was constructed as shown in red in Fig. 17.

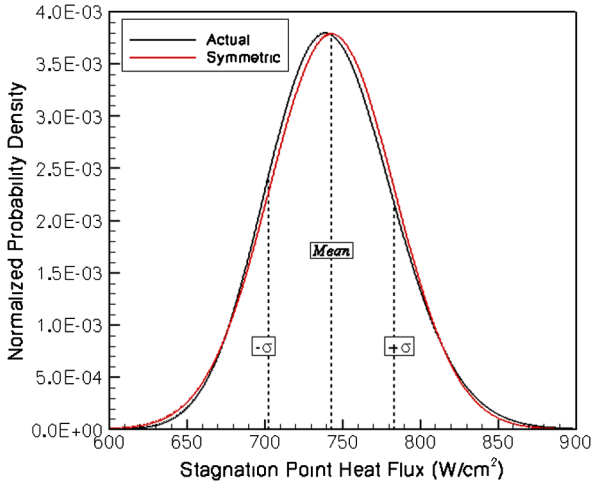

Fig. 17 Surface heat flux PDF because of N_2-N collision integral coefficient variation.

V. Conclusions

The PCE has been applied for UQ analyses of hypersonic CFD calculations for a typical blunt-body at reentry conditions. A verification of the PCE implementation is carried out by comparison with the MC sampling for a Fay–Riddell stagnation point heat flux correlation and the third-order PCE expansion has been determined to give sufficient accuracy. The third-order PCE analysis has been applied to hypersonic flow simulations for a FIRE 2 configuration. Input parameters such as freestream conditions and collision integral coefficients were varied, and their effect on the surface heating and flowfield properties were analyzed.

Grid adaptation effects on the flowfield properties of interest were determined to be negligible. Allowing the baseline grid to adapt for the -10% variation in freestream density had resulted in only small differences in surface heat flux within a region measuring 15% of the total length.

Varying the density had maximum uncertainties in surface heat flux both in the shoulder region and at the stagnation point. Translational temperature and static pressure had higher uncertainty levels before the shock along the stagnation streamline, but only the translational temperature also had an even higher uncertainty after the shock. Skewness calculations indicate that mean surface heat fluxes are being underpredicted for freestream density variations.

For freestream temperature variations, there was little effect. Flowfield properties were most insensitive to this parameter, as the relative uncertainty is 2 orders of magnitude less than the input uncertainty.

When freestream velocity was varied, the uncertainty in surface heating was much higher than the input uncertainty, and the maximum was located in the shoulder region where the velocity gradients at the wall are smaller. Higher translational temperature and static pressure uncertainties are likewise located in the shoulder region, but have maxima in the shock near the outflow boundary. Positive values in surface heat flux skewness indicate overpredictions due to freestream velocity variations.

Collision integral coefficient variations had maximum uncertainty levels in surface heat flux in the region between stagnation point and the shoulder. The boundary layer had contained the highest concentration of nitrogen molecule and atom pairs, and therefore the maximum uncertainty in translational temperature and static pressure was located within the boundary layer. The lower sensitivity to this parameter in comparison to Palmer [4] is thought to be due to the differences in the number of collision pairs varied. A test would be to vary two collision pairs simultaneously and ascertain whether the uncertainty levels are significantly effected or not. Surface heat flux skewness calculations show both over and underpredictions are present; with the maximum magnitude being 1.3 at the outflow of the shoulder.

The findings of this study indicate that the PCE methods can provide useful analyses of practical hypersonic CFD problems. The efficient calculation of the higher-order moments by PC method is beneficial for assessing confidence levels of high-fidelity aeroheating simulations.

Acknowledgments

This research was supported by U.S. Air Force Research Laboratory/Aeronautical Sciences Division, Computational Sciences Branch (RBAC) summer research program. The authors would like to thank Eswar Josyula of U.S. Air Force Research Laboratory/RBAC for his support of this research. The authors would also like to thank Alireza Mazaheri of NASA Langley for his help with LAURA and Venkattraman Ayyaswamy of Purdue University for his assistance with PDF construction from PCE.

References

[1] Ouzts, P., "The Joint Technology Office on Hypersonics," *Proceedings of 15th AIAA International Space Planes and Hypersonic Systems and Technologies Conference*, 2008; also AIAA Paper 2008-2576.

[2] Falempin, F., "Possible Military Application of High-Speed Airbreathing Propulsion in the 21st Century: An European Vision," *Proceedings of AIAA International Air and Space Symposium and Exposition: The Next 100 Years*, 2003; also AIAA Paper 2003-2723.

[3] Bose, D., Wright, M., and Palmer, G., "Uncertainty Analysis of Laminar Aeroheating Predictions for Mars Entries," *Journal of Thermophysics and Heat Transfer*, Vol. 20, No. 4, 2006, p. 652. doi:10.2514/1.20993

[4] Palmer, G. E., "Uncertainty Analysis of CEV LEO and Lunar Return Entries," *Proceedings of the 39th AIAA Thermophysics Conference*, 2007; also AIAA Paper 2007-4253.

[5] Xiu, D., and Karniadakis, G., "Modeling Uncertainty in Flow Simulations via Generalized Polynomial Chaos," *Journal of Computational Physics*, Vol. 187, No. 1, 2003, pp. 137–167. doi:10.1016/S0021-9991(03)00092-5

[6] Hosder, S., and Walters, R. W., "Non-Intrusive Polynomial Chaos Methods for Uncertainty Quantification in Fluid Dynamics," *48th AIAA Aerospace Sciences Meeting*, 2010; also AIAA Paper 2010-129.

[7] Nobile, F., Tempone, R., and Wesbster, C., "A Sparse Grid Stochastic Collocation Method for Partial Differential Equations with Random Input Data," *SIAM Journal on Numerical Analysis*, Vol. 46, No. 5, 2008, pp. 2309–2345. doi:10.1137/060663660

[8] Witteveen, J. A., and Iaccarino, G., "Simplex Elements Stochastic Collocation for Uncertainty Propagation in Robust Design Optimization," *48th AIAA Aerospace Sciences Meeting*, 2010; also AIAA Paper 2010-1313.

[9] Champion, K. S. W., "Middle Atmosphere Density Data and Comparison With Models," *Advances in Space Research*, Vol. 10, No. 6, 1990, pp. (6)17–(6)26.

[10] Roy, C. J., and Oberkampf, W. L., "A Complete Framework for Verification, Validation, and Uncertainty Quantification in Scientific Computing," *48th AIAA Aerospace Sciences Meeting*, 2010; also AIAA Paper 2010-124.

[11] Cornette, E. S., "Forebody Temperatures and Calorimeter Heating Rates Measured During Project FIRE 2 Reentry at 11.35 Kilometers Per Second," NASA TM X-1305, NASA Langley Research Center, Nov. 1966.

[12] Abramowitz, M., and Stegun, I. A., *Handbook of Mathematical Functions with Formulas, Graphs, and Mathematical Tables*, 9th ed., Dover, New York, 1972, pp. 771–802.

[13] Greenwood, R., and Miller, J., "Zeros of the Hermite Polynomials and Weights for Gauss' Mechanical Quadrature Formula," *Bulletin (New Series) of the American Mathematical Society*, Vol. 54, No. 8, 1948, pp. 765–769. doi:10.1090/S0002-9904-1948-09075-9

[14] Najm, H. N., "Uncertainty Quantification and Polynomial Chaos Techniques in Computational Fluid Dynamics," *Annual Review of Fluid Mechanics*, Vol. 41, No. 1, 2009, pp. 35–52. doi:10.1146/annurev.fluid.010908.165248

[15] Gupta, R. N., Yos, J. M., Thompson, R. A., and Lee, K.-P., "A Review of Reaction Rates and Thermodynamic and Transport Properties for an 11-Species Air Model for Chemical and Thermal Nonequilibrium Calculations to 30,000 K," NASA RP-1232, 1990.

[16] Hillje, E., "Entry Flight Aerodynamics from Apollo Mission AS-202," NASA TN D-4185, 1965.

[17] Hash, D., Olejniczak, J., Wright, M., Pulsonetti, D. P. M., Hollis, B., Gnoffo, P., Barnhardt, M., Nompelis, I., and Candler, G., "FIRE 2 Calculations for Hypersonic Nonequilibrium Aerothermodynamics Code Verification: DPLR, LAURA, and US3D," *45th AIAA Aerospace Sciences Meeting and Exhibit*, 2007; also AIAA Paper 2007-605.